analytical chemistry

pubs.acs.org/ac Article

Nanoconfined Cathodic Electrochemiluminescence for Self-Sensitized Bioimaging of Membrane Protein

Siqi Yu, Xiangfu Hu, Jianbin Pan, Jianping Lei, and Huangxian Ju*

Cite This: *Anal. Chem.* 2023, 95, 16593−16599 Read Online

ACCESS | Metrics & More | Article Recommendations | Supporting Information

ABSTRACT: Self-enhanced electrochemiluminescence (ECL) can be achieved via the confinement of coreactants and ECL emitters in a single nanostructure. This strategy has been used for the design of anodic ECL systems with amine compounds as coreactants. In this work, a novel confinement system was proposed by codoping positively charged ECL emitter tris(2,2′-bipyridine)ruthenium(II) ($Ru(bpy)_3^{2+}$) and negatively charged coreactant peroxydisulfate ($S_2O_8^{2-}$) in silica nanoparticles. The codoping process could be performed by introducing $S_2O_8^{2-}$ in cationic poly(diallyldimethylammonium chloride) (PDDA) to form PDDA@$S_2O_8^{2-}$ and then encapsulating it and $Ru(bpy)_3^{2+}$ in the Triton X-100 vesicle followed by the hydrolysis of tetraethyl ortosilicate, surface modification, and demulsification. The obtained RuSSNs exhibited good homogeneity, excellent monodispersity, acceptable biocompatibility, and 2.9-fold stronger ECL emission than $Ru(bpy)_3^{2+}$-doped silica nanoparticles at an equal amount of nanoparticles in the presence of 0.1 M $K_2S_2O_8$. Thus, an in situ self-sensitized cathodic ECL imaging method was designed for the monitoring of glycoprotein on living cell membranes. This work provides a new way for the modification, enhancement, and application of nano-ECL emitters in biological analysis.

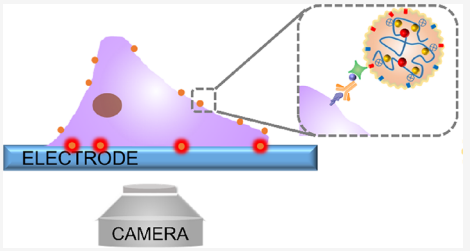

INTRODUCTION

Electrochemiluminescence (ECL) is a light-emitting process, in which the excited state species are generated via exergonic electron transfer in the vicinity of the working electrode and then transit to the ground state to emit photons.[1] Different from the traditional intensity measurement with a photomultiplier tube in a dark box, ECL imaging is performed with a charge-coupled device (CCD) camera for optical readout.[2,3] It has become a powerful tool in cell analysis,[3−5] electrocatalytic investigation of single nanoparticles,[6,7] ECL mechanism exploration,[8−10] and biosensing.[11] In single-cell imaging, the ECL-emitting thickness can be well tuned by altering the concentration ratio of ECL emitters to coreactants and the type of coreactants with distinct lifetime of radicals,[4,12] which is different from the traditional photoluminescence imaging where all the labeled targets in the field are illuminated. At a high concentration of coreactants with a short lifetime of radicals, the thickness can be as thin as ∼500 nm due to the characteristic surface-confined ECL mechanism,[3,13] which is the same as the characteristic of total internal reflection fluorescence (TIRF) microscopy. Thus, ECL imaging can reveal the detailed cell-matrix adhesions, which cannot be resolved by the classic fluorescence microscopy.[14] An emission layer thickness of ∼10 μm can even be achieved via a "catalytic route" at a high ECL emitter concentration and low coreactant concentration,[15] which allows the observation of intracellular hierarchical structures without the need of multiple labels. In addition, the passive transport process of substances across the membrane can be revealed through the diffusion of coreactants.[4] However, the ECL emitters with a strong emission signal remain urgently needed in CCD-based ECL imaging.

Recently, the nanoconfinement effects of metal−organic frameworks (MOFs), mesoporous silica nanoparticles, and zeolite have attracted considerable attention in the design of sensitive ECL imaging methods,[13,16−18] and some super-resolution imaging techniques, such as single-molecular localization microscopy[11,19−21] and super-resolution radial fluctuations (SRRF),[6] have also been combined with ECL imaging to achieve high spatial resolution. These ECL imaging methods generally use anodic ECL emission of the tris(2,2′-bipyridine)ruthenium(II) ($Ru(bpy)_3^{2+}$)/tri-*n*-propylamine (TPA) system as the signal source.[3,4,13,16−18] This system needs exogenous coreactant TPA, which is environmentally hazardous[22] and not user-friendly.[23] Through confining the ECL emitter and coreactant in a single nanostructure such as polymer dots (Pdots),[24] amine-rich nitrogen-doped carbon nanodots (NCNDs),[25] mixed-ligand MOFs,[26] and lipoic acid Au nanoclusters,[27] some self-enhanced anodic ECL systems have been proposed to achieve strong ECL emission without the need of exogenous coreactants. To avoid the interference of some biomolecules with redox activity in the anodic

Received: June 22, 2023
Revised: September 15, 2023
Accepted: October 11, 2023
Published: October 30, 2023

https://doi.org/10.1021/acs.analchem.3c02726
Anal. Chem. 2023, 95, 16593−16599

Scheme 1. Schematic Representation of the Synthesis of $S_2O_8^{2-}$ and $Ru(bpy)_3^{2+}$-Codoped Silica Nanoparticles (bRuSSNs) and Amino-Functionalized bRuSSNs (RuSSNs) As Well As ECL Imaging of Cell Membrane Protein EGFR with SA@RuSSNs

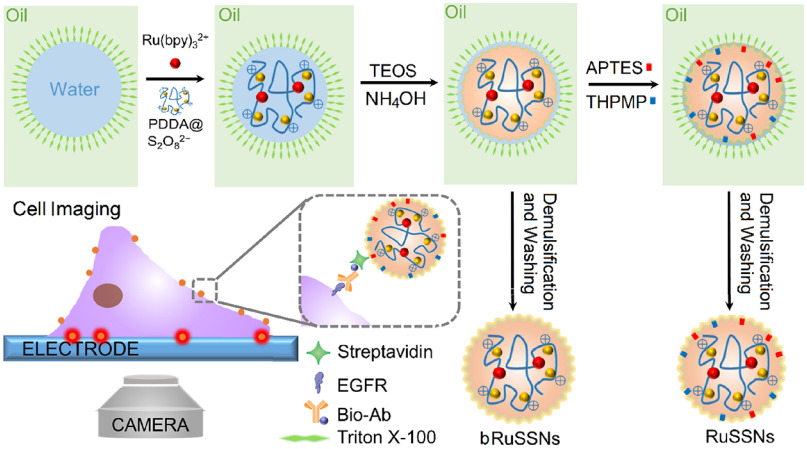

potential region,[15,28,29] it is necessary to develop a cathodic ECL confinement system.

Different from most anodic coreactants, the general cathodic coreactants such as peroxydisulfate ($S_2O_8^{2-}$) and hydrogen peroxide (H_2O_2) cannot directly bind to the emitters for the design of confinement systems, though the in situ production strategies of $S_2O_8^{2-}$[30] and H_2O_2[31] at the boron-doped diamond electrode have been proposed for avoiding the addition of exogenous coreactants. To solve the problem described above, this work proposed a cathodic ECL confinement system by codoping $Ru(bpy)_3^{2+}$ and $S_2O_8^{2-}$ in silica nanoparticles, which can facilitate the subsequent biological coupling reaction[32] and have been used for the doping of positively charged dyes[33,34] owing to the presence of negatively charged silanol groups.[35] The codoping process was conveniently performed by introducing $S_2O_8^{2-}$ in cationic poly(diallyldimethylammonium chloride) (PDDA) to form PDDA@$S_2O_8^{2-}$ and then encapsulating it and $Ru(bpy)_3^{2+}$ in a Triton X-100 vesicle followed by the hydrolysis of tetraethyl ortosilicate (TEOS), surface modification, and demulsification (Scheme 1). The obtained RuSSNs showed the ECL emission to be 2.9 times stronger than that of $Ru(bpy)_3^{2+}$-doped silica nanoparticles (RuSNs) at an equal amount of nanoparticles in the presence of 0.1 M $K_2S_2O_8$. Thus, a self-sensitized cathodic ECL imaging method was proposed for single-cell membrane protein analysis with the epidermal growth factor receptor (EGFR) as the target model. The proposed confinement strategy is expected to be applicable to other ECL emitters.

EXPERIMENTAL SECTION

Materials, Reagents, and Apparatus. The detailed information is described in the Supporting Information.

Preparation of Bare RuSSNs (bRuSSNs) and RuSSNs. PDDA@$S_2O_8^{2-}$ was first prepared by mildly stirring 5.0 mL of solution containing 20 mg mL^{-1} PDDA and 50 mg of $K_2S_2O_8$ at room temperature for 20 min (Scheme S1). $Ru(bpy)_3Cl_2 \cdot 6H_2O$ (3 mg) was then added in 500 μL of the as-prepared PDDA@$S_2O_8^{2-}$ solution, which was mixed with 7.5 mL of cyclohexane, 1.6 mL of *n*-hexanol, and 1.77 mL of polyethylene glycol *tert*-octylphenyl ether (Triton X-100) to stir for 15 min at room temperature. Afterward, 100 μL of tetraethyl ortosilicate (TEOS) was added in the mixture to stir for 30 min, and then 60 μL of aqueous ammonia solution (NH_4OH) (25−28 wt % in H_2O) was introduced to initiate the hydrolysis of TEOS for 12 h under stirring. After the product was mixed with 10 mL of acetone for demulsification and centrifuged at 12,000 rpm for 10 min,[36] and the sediment was washed with ethanol and water several times to remove the free surfactant, the resultant bRuSSNs were redispersed in 10 mL of water for further use.

RuSSNs were prepared by mixing the above product with 40 μL of 3-(trihydroxysilyl)propyl methylphosphonate (THPMP) and 10 μL of 3-aminopropyltriethoxysilane (APTES) for surface amino modification with stirring for 4 h at room temperature and then demulsification with 10 mL of acetone to centrifuge at 12,000 rpm for 10 min (Scheme 1).

Preparation of Bare RuSNs (bRuSNs) and RuSNs. The bRuSNs were prepared by mixing 500 μL of 6 mg mL^{-1} $Ru(bpy)_3Cl_2 \cdot 6H_2O$ with 7.5 mL of cyclohexane, 1.6 mL of *n*-hexanol, and 1.77 mL of Triton X-100 to stir for 15 min at room temperature and then 100 μL of tetraethyl ortosilicate (TEOS) to stir for 30 min, which was introduced with 60 μL of NH_4OH (25−28 wt % in H_2O) to initiate the hydrolysis of TEOS for 12 h. After the product was mixed with 10 mL of acetone for demulsification and centrifuged at 12,000 rpm for 10 min, and the sediment was washed with ethanol and water several times to remove the free surfactant, the resultant bRuSNs were redispersed in water for further use. The surface modification and demulsification of bRuSNs were performed to obtain RuSNs by the same process described above.

Estimation of Ru^{2+} and $S_2O_8^{2-}$ Numbers in Single Nanoparticles and Concentrations in RuSNs and RuSSNs Dispersions. First, the volumes of spherical RuSNs and RuSSNs were calculated with the transmission electron microscopic (TEM) diameters to obtain the average weights of each nanoparticle with a tabulated SiO_2 density of 2.2 g cm^{-3}. Then, the molar ratios of Ru^{2+} to SiO_2 and $S_2O_8^{2-}$ to SiO_2 could be calculated from the inductively coupled plasma atomic emission spectroscopy (ICP-AES) results. The numbers of Ru^{2+} and $S_2O_8^{2-}$ in a single nanoparticle were thus acquired.

The absorption spectra were used to determine the concentrations of Ru^{2+} in RuSNs and RuSSNs dispersions, assuming the same molar excitation coefficient ε of Ru^{2+} embedded in the silica lattice as that of 14,600 cm^{-1} M^{-1} at 452 nm in solution. The concentration of $S_2O_8^{2-}$ in RuSSNs dispersion was obtained from the molar ratio of Ru^{2+} to $S_2O_8^{2-}$, which was calculated from the ICP-AES measure-

https://doi.org/10.1021/acs.analchem.3c02726
Anal. Chem. 2023, 95, 16593−16599

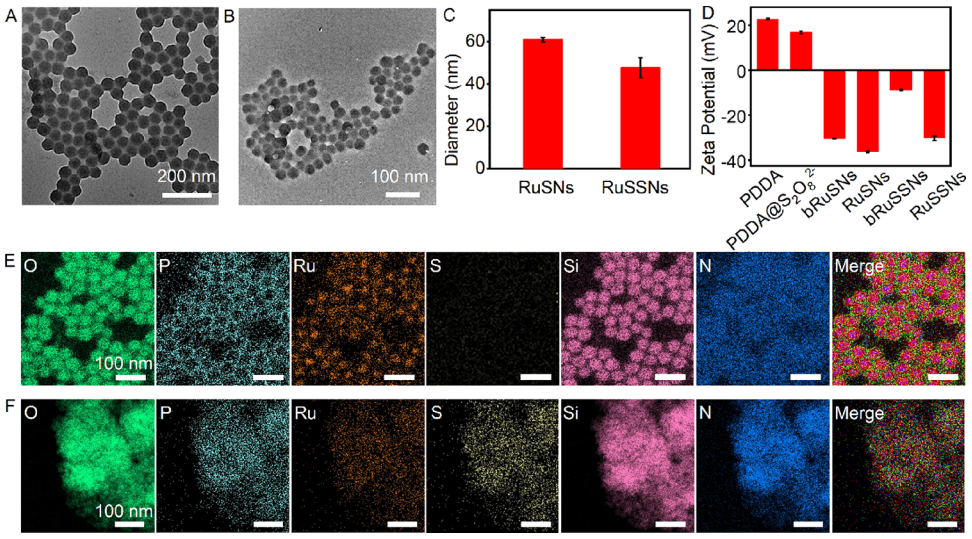

Figure 1. (A, B) TEM images of RuSNs (A) and RuSSNs (B). (C) Hydrodynamic diameters of RuSNs and RuSSNs. (D) Zeta potentials of 20 mg mL^{-1} PDDA, PDDA@$S_2O_8^{2-}$, bRuSNs, RuSNs, bRuSSNs, and RuSSNs dispersions. (E, F) EDX elemental mapping images of RuSNs (E) and RuSSNs (F).

ments. Accordingly, the concentrations of nanoparticles in RuSNs and RuSSNs dispersions were calculated by dividing the concentrations of Ru^{2+} in the dispersions with the amounts of Ru^{2+} in a single nanoparticle.

Electrode Modification. Glassy carbon electrodes (GCEs) were first polished with 0.3 and 0.05 μm alumina slurries sequentially and sonicated in ethanol and distilled water for 3 min. After the electrodes were dried with a steam of high-purity nitrogen, 10 μL of bRuSNs, RuSNs, bRuSSNs, or RuSSNs dispersion was individually cast on their surface and dried under ambient conditions to get the bRuSNs-, RuSNs-, bRuSSNs-, or RuSSNs-modified GCEs.

Preparation of Streptavidin-Conjugated RuSSNs (SA@RuSSNs). According to the previous report,[24] 100 μL of RuSSNs dispersion was mixed with 200 μL of H_2O, 6 μL of 1 M 4-(2-hydroxyethyl)-1-piperazineethanesulfonic acid (HEPES), 20 μL of 0.1 M NaOH, 6 μL of polyethylene glycol (PEG, 5% w/v, Mw = 3350), 6 μL of 5 mg mL^{-1} 1-(3-(dimethylamino)propyl)-3-ethylcarbodiimide hydrochloride (EDC), and 10 μL of 2 mg mL^{-1} streptavidin (SA) and stirred overnight at 30 °C. Afterward, 6 μL of bovine serum albumin (BSA, 10 wt %) was added in the mixture for another 30 min. The resulting SA@RuSSNs were washed with 300 μL of 0.01 M pH 7.4 phosphate buffer solution (PBS) three times, dispersed in 200 μL of 0.01 M pH 7.4 PBS, and stored at 4 °C for further use.

Cell Culture and Recognition of SA@RuSSNs. A431 and MCF-7 cells were cultured in DMEM and RPMI-1640 media, respectively, supplemented with 10% FBS and 100 μg mL^{-1} penicillin−streptomycin at 37 °C in a humidified atmosphere containing 5% CO_2 to maintain a density between 5×10^5 and 2×10^6 cells mL^{-1}. At the logarithmic growth phase, the cells were trypsinized and washed twice with sterile 0.01 M pH 7.4 PBS by centrifugation at 1000*g* for 10 min, which were then resuspended in 0.01 M pH 7.4 PBS containing 1.0 mM Ca^{2+} and 1.0 mM Mg^{2+} to obtain homogeneous cell suspensions.

After 200 μL of 5×10^5 cells mL^{-1} A431 and MCF-7 cell suspensions were incubated with 1 μL of 1 mg mL^{-1} biotin-labeled EGFR antibody (Bio-Ab) on a rotary shaker in the dark for 45 min at 37 °C, and these cells were redispersed in 200 μL of SA@RuSSNs dispersions and shaken in the dark for 45 min at 37 °C. These SA@RuSSNs-treated A431 and MCF-7 cells were then redispersed in DMEM or RPMI-1640 media with 10% FBS and 100 μg mL^{-1} penicillin−streptomycin, respectively, and seeded on indium tin oxide (ITO) electrodes to incubate overnight at 37 °C in a humidified atmosphere containing 5% CO_2 for ECL imaging.

ECL Imaging. The ECL imaging system was assembled with an inverted microscope (DMI8, Leica, Germany) and an electron multiplying charge-coupled device (EM-CCD) (iXon Ultra, Andor, UK) as the microscopic imaging module and a CHI-660D electrochemical workstation as the electrochemical initiation module. The homemade ECL imaging cell was used in a three-electrode configuration, in which the self-fabricated ITO sides acted as the working electrode, a Ag/AgCl wire as the reference electrode, and a Pt wire as the counter electrode. The ECL images were recorded in the amperometric *i*−*t* mode at −1.45 V with an exposure time of 20 s.

Cytotoxicity and Viability Assay. The cytotoxicity of SA@RuSSNs was evaluated with a conventional cell counting kit-8 (CCK-8) assay by seeding 200 μL of 5×10^4 cells mL^{-1} pristine A431 cells and SA@RuSSN-treated A431 cells in each well of a 96-well plate to culture overnight and then adding 10 μL of the CCK-8 reagent in the well to incubate at 37 °C for 2 h. The absorbance values were used to calculate the viability of these cells.

To explore the effect of the applied potential on cell viability, a potential of +1.2 or −1.45 V (vs Ag/AgCl) was applied at 200 μL of 1.75×10^6 cells mL^{-1} A431 cell-seeded FTO slide in 0.01 M pH 7.4 PBS containing 1.0 mM Ca^{2+} and 1.0 mM Mg^{2+} for 0, 30, 60, 90, 120, 180, and 240 s. Afterward, these cells were twice washed with 0.01 M pH 7.4 PBS and then co-stained with 200 μL of 0.01 M pH 7.4 PBS containing 2.0 μM Calcein AM and 8.0 μM PI at 37 °C for 20 min and washed with 0.01 M pH 7.4 PBS three times. The viability assay was performed in 0.01 M pH 7.4 PBS containing 1.0 mM Ca^{2+} and 1.0 mM Mg^{2+} with an inverted fluorescence microscope (DMI8, Leica, Germany). The wavelengths for excitation/

https://doi.org/10.1021/acs.analchem.3c02726
Anal. Chem. 2023, 95, 16593−16599

Table 1. Numbers of Ru^{2+} and $S_2O_8^{2-}$ per Nanoparticle, Diameters from TEM, Hydrodynamic Diameters, Zeta Potentials, and PL and ECL Emission Wavelengths of RuSNs and RuSSNs

sample	$n_{Ru2+/NP}$	$n_{S2O82^-/NP}$	d_{NP} (nm)	d_H (nm)	zeta potential (mV)	$\lambda_{em,\ PL}$(nm)	$\lambda_{em,\ ECL}$(nm)
RuSNs	1.6×10^4		46	60	−37.7	622	659
RuSSNs	3.9×10^3	2.0×10^4	32	47	−31.4	607	641

emission of Calcein AM and PI were 495/520 and 530/620 nm, respectively.

RESULTS AND DISCUSSION

Characterization of RuSNs and RuSSNs. The TEM images showed good monodispersity and excellent uniformity of both RuSNs and RuSSNs with diameters of 46 and 32 nm, respectively (Figure 1A,B and Table 1), which were consistent with 46 and 30 nm observed with atomic force microscopy (AFM), respectively (Figure S1). The dynamic light scattering (DLS) measurements displayed average hydrated ionic diameters of 60 and 47 nm for RuSNs and RuSSNs, respectively (Figure 1C). After $S_2O_8^{2-}$ was conjugated in PDDA, the zeta potential changed from 23.7 to 17.6 mV (Figure 1D). The bRuSNs and bRuSSNs presented negatively charged surfaces due to the presence of silanol groups,[35] leading to zeta potentials of −31.6 and −9.1 mV, respectively. However, the zeta potentials of RuSNs and RuSSNs negatively shifted to −37.8 and −31.1 mV, respectively (Table 1), which resulted from the presence of negatively charged methylphosphonate groups from THPMP. Compared with RuSNs or bRuSNs, the zeta potential of RuSSNs or bRuSSNs was more positive, which was attributed to the introduction of positively charged PDDA@$S_2O_8^{2-}$. The energy-dispersive X-ray spectroscopy (EDX) elemental mapping images of RuSNs verified the coexistence of O, P, Ru, Si, and N elements and the absence of the S element (Figure 1E). The presence of P and N elements was associated with the modification of THPMP and APTES. In RuSSNs, the content of the S element became distinct (Figure 1F) due to the doping of PDDA@$S_2O_8^{2-}$. These results indicated the successful codoping of $Ru(bpy)_3^{2+}$ and $S_2O_8^{2-}$ into RuSSNs and surface amino modification.

Ru^{2+} and $S_2O_8^{2-}$ Amounts in RuSNs and RuSSNs. The absorbance spectra of $Ru(bpy)_3^{2+}$, RuSNs, and RuSSNs at different concentrations were recorded for the determination of the amounts of $Ru(bpy)_3^{2+}$ in RuSSNs and RuSNs (Figure S2A). The amount of $S_2O_8^{2-}$ in single RuSSNs was obtained from the molar ratio of Ru^{2+} to $S_2O_8^{2-}$, which was obtained from ICP-AES measurements (Table S1). The average numbers of $Ru(bpy)_3^{2+}$ and $S_2O_8^{2-}$ in single RuSSNs were estimated to be $\sim 3.9 \times 10^3$ and 2.0×10^4, respectively, and the number of $Ru(bpy)_3^{2+}$ in single RuSNs was $\sim 1.6 \times 10^4$ (Table 1). Thus, the concentrations of $Ru(bpy)_3^{2+}$ and $S_2O_8^{2-}$ in the dispersion of RuSSNs were 115 and 608 μM, respectively.

Electrochemical and Photophysical Properties of RuSNs and RuSSNs. The electrochemical properties of RuSNs and RuSSNs in 0.1 M PBS were investigated at first. At both RuSNs/GCE and RuSSNs/GCE, a reduction peak of $Ru(bpy)_3^{2+}$ could be observed at −1.40 V (Figure S2B and inset in Figure 2A),[37] similar to that of 115 μM $Ru(bpy)_3^{2+}$ at the bare GCE, while the nanoconfined $S_2O_8^{2-}$ did not show obvious response due to its limited amount on the electrode, just as that of 608 μM $K_2S_2O_8$ at the bare GCE (Figure S3). In the presence of 0.1 M $K_2S_2O_8$, the reduction wave of RuSNs/GCE was overlapped and a distinct reduction peak appeared at −0.90 V (Figure 2A), which was related to the production of a

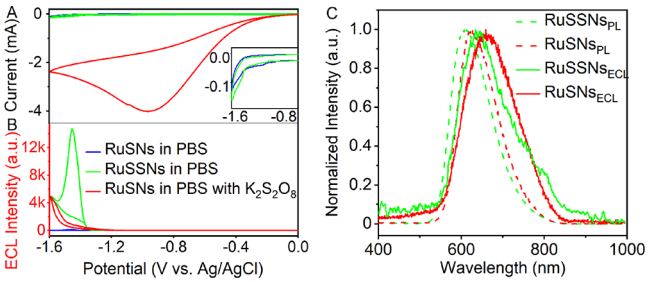

Figure 2. (A) CVs of RuSNs/GCE (blue line) and RuSSNs/GCE (green line) in 0.1 M PBS and RuSNs/GCE in 0.1 M PBS containing 0.1 M $K_2S_2O_8$ (red line) after N_2 bubbling for 30 min at an equal amount of nanoparticles. Inset in panel (A): Enlargement of CV curves. (B) ECL curves under the same conditions as those in panel (A). (C) PL (dashed lines) and ECL (solid lines) spectra of RuSNs (red lines) and RuSSNs (green lines).

strongly oxidizing intermediate $SO_4^{\cdot-}$.[38] In the absence of $K_2S_2O_8$, RuSNs/GCE showed negligible ECL emission, while strong ECL emission appeared at RuSSNs/GCE (Figure 2B), indicating the importance of $K_2S_2O_8$ as an efficient coreactant for generating excited state $Ru(bpy)_3^{2+*}$ via the electron transfer between electrogenerated $Ru(bpy)_3^{+}$ and $SO_4^{\cdot-}$.[37] Interestingly, the cathodic ECL peak of RuSSNs/GCE was not only stronger but also more positive than that of RuSNs/GCE in the presence of 0.1 M $K_2S_2O_8$ (Figure 2B). The negative shift of ECL potential could be attributed to the diffusion of $S_2O_8^{2-}$ and $SO_4^{\cdot-}$ and the electrostatic repulsion between anionic species and negatively charged RuSNs (Figure 1D) in the RuSNs/$S_2O_8^{2-}$ system,[25,32] which was different from the electron hopping mechanism in RuSSNs (see below).[34] The ECL intensity of RuSSNs at −1.45 V was 2.9 times higher than that of RuSNs/$K_2S_2O_8$ at an equal amount of nanoparticles (10 μL of 30 nM; Table 1) at −1.60 V, indicating that the codoping of the coreactant was beneficial to the electron transfer between electrogenerated intermediates and the enhancement of ECL emission.

Considering the ion balance, the amount of $K_2S_2O_8$ conjugated in PDDA was optimized to be 50 mg of $K_2S_2O_8$ for 5.0 mL of 20 mg mL^{-1} PDDA (Figure S4). The optimal modification time of APTES and THPMP was 4 h, at which the RuSSNs retained 90% of the ECL intensity of bRuSSNs (Figure S5). A longer modification time resulted in an excessively large size due to the presence of TEOS, which was adverse to the electron transfer from the electrode to codoped $Ru(bpy)_3^{2+}$ and $S_2O_8^{2-}$ and the electron hopping between redox centers,[32,33] thus greatly decreasing the ECL intensity. In addition, RuSSNs maintained over 90% of the initial ECL intensity after storage at 4 °C for 2 weeks (Figure S6), demonstrating acceptable stability of RuSSNs for bioanalysis. The decay of ECL intensity after a stepping pulse could be attributed to the consumption of coreactant (Figure S7).

The photoluminescence (PL) emissions of RuSNs and RuSSNs centered at 622 and 607 nm, respectively, while their ECL emission peaks were located at 659 and 641 nm,

https://doi.org/10.1021/acs.analchem.3c02726
Anal. Chem. 2023, 95, 16593−16599

respectively (Figure 2C and Table 1). It was worth noting that the bathochromic shift of the maximum ECL emission wavelength compared to PL emission was associated with the inner-filter effect.[39]

ECL Mechanism. Compared to RuSNs, doping $S_2O_8^{2-}$ slightly increased the electron transfer impedance due to the presence of PDDA (Figure 3A). However, the ECL intensity of

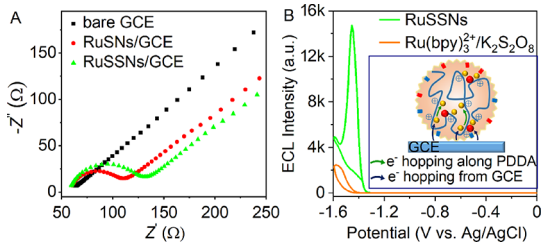

Figure 3. (A) EIS Nyquist plots of bare and modified GCEs in 0.1 M KCl containing 5 mM $K_4[Fe(CN)_6]/K_3[Fe(CN)_6]$ (1:1) in the frequency range from 0.01 Hz to 10 kHz with a potential amplitude of 10 mV. (B) ECL curves of RuSSNs/GCE (green line) in 0.1 M PBS and bare GCE in 0.1 M PBS containing 115 μM $Ru(bpy)_3^{2+}$ and 608 μM $K_2S_2O_8$ (orange line) after N_2 bubbling for 30 min. Inset: Electron hopping from the electrode and along the PDDA chain inside RuSSNs.

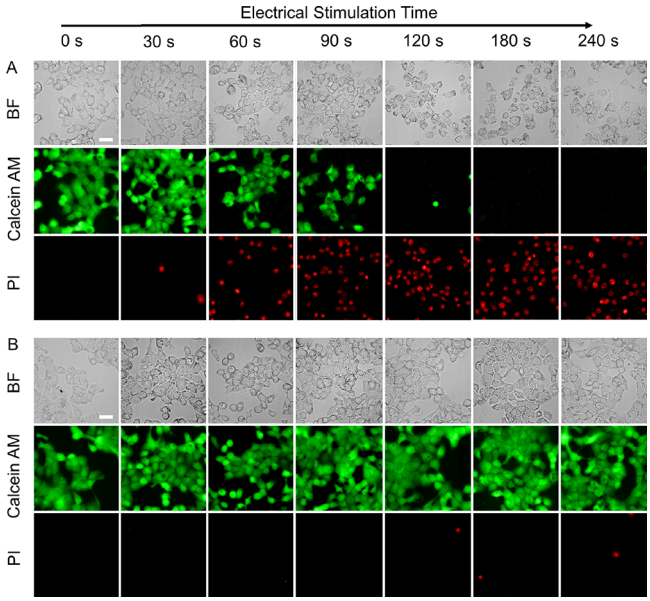

Figure 4. BF and FL images of A431 cells in 0.01 M pH 7.4 PBS containing 1.0 mM Ca^{2+} and 1.0 mM Mg^{2+} after applying (A) +1.2 V and (B) −1.45 V (vs. Ag/AgCl) for 0−240 s and then staining with Calcein AM (green) and PI (red). Scale bars: 20 μm.

RuSSNs/GCE at −1.45 V was 6-fold stronger than that of the $Ru(bpy)_3^{2+}$ (115 μM)/$S_2O_8^{2-}$ (608 μM) system with the same amount of $Ru(bpy)_3^{2+}$ and $S_2O_8^{2-}$ at a peak potential of −1.57 V (Figure 3B). The self-enhanced cathodic ECL emission of RuSSNs could be attributed to the following reasons. First, the nanoconfinement of $Ru(bpy)_3^{2+}$ and $S_2O_8^{2-}$ in RuSSNs restricted the diffusion of electrogenerated radical intermediates and thus protected the radical species from oxygen and water quenching and the self-quenching to achieve minor energy loss.[25,32] Second, the electron transfer reactions were more efficient in RuSSNs compared to RuSNs/$S_2O_8^{2-}$ or $Ru(bpy)_3^{2+}$/$S_2O_8^{2-}$ due to the facilitated electron hopping between nanoconfined redox centers (inset in Figure 3B).[34] Third, in the RuSNs/$S_2O_8^{2-}$ system, the free anionic radical intermediate $SO_4^{\cdot-}$ was difficult to approach the surface of the overall negatively charged RuSNs due to the electrostatic repulsion.[32] Finally, the positively charged PDDA could stabilize the adjacent coreactant anionic radicals $SO_4^{\cdot-}$, which was beneficial for the ECL emission.[40,41]

Tolerance of A431 Cells to External Electrical Stimulation. To elucidate the importance of the cathodic ECL confinement system in cell analysis, the tolerance of A431 cells to external electrical stimulation was examined by applying the potentials of +1.20 and −1.45 V vs. Ag/AgCl to the cell-seeded electrodes. At the applied potentials, the $Ru(bpy)_3^{2+}$/TPA system showed the anodic ECL emission peak,[32] while RuSSNs/GCE showed the cathodic ECL peak. After applying a potential of +1.20 V for 60 s, the BF images showed obvious cell membrane damage and an unclear cell outline (Figure 4A). The fluorescence images of the cells stained with Calcein AM (green) and PI (PI) also showed the decrease in live cells and the increase in dead cells with the increasing electrical stimulation time. By contrast, the cells stimulated at −1.45 V maintained a good living state even after 240 s (Figure 4B), and the dead cells hardly appeared, which could be attributed to the negatively charged lipid bilayer of the cell membrane. Therefore, the cathodic ECL confinement system is promising in ECL analysis of live cells.

ECL Imaging of Membrane Protein. To achieve the in situ ECL imaging of membrane protein, RuSSNs were first covalently linked with SA to obtain SA@RuSSNs, which was verified with Cy3-labeled SA (Cy3-SA). Both Cy3-SA and the Cy3-SA@RuSSNs showed similar PL emissions, which were completely different from RuSSNs (Figure S8). The cytotoxicity of SA@RuSSNs was evaluated with the conventional cell counting kit-8 (CCK-8) assay, which indicated negligible toxicity of SA@RuSSNs to A431 cells (Figure S9).

EGFR as a transmembrane glycoprotein is often overexpressed in tumors[42] and can be activated via binding with ligands such as EGF to result in changes of the signaling pathway in cells.[43] It is related to the cell proliferation, angiogenesis, tumor invasion, and cell apoptosis. Using EGFR overexpressed on A431 cells as the target model, SA@RuSSNs were first bound to A431 cells by incubating the cells with the biotin-labeled EGFR antibody and then SA@RuSSNs. The in situ cathodic ECL imaging of EGFR on live cells was then performed. Due to the nanoconfinement of $Ru(bpy)_3^{2+}$ and $S_2O_8^{2-}$ in RuSSNs, the self-sensitized ECL emission was generated on the cells adhered on the ITO electrode in 0.1 M PBS, and the emission region basically covered the entire contact area between the cells and electrode (Figure 5A,C), which was consistent with the result obtained after Triton X-100 permeable treatment of cells.[4] Compared to the PL imaging (Figure 5B and Figure S10B), the ECL imaging with RuSSNs possessed higher sensitivity and allowed visualizing a larger range of the cell border (Figure 5C and Figure S10C). The specificity of the proposed imaging method was further demonstrated by using MCF-7 cells, which express EGFR lowly on the membrane, as the control. As expected, both the PL and the ECL images showed negligible spots (Figure 5D−F), indicating the reliability of the in situ ECL imaging method with RuSSNs as the emitter.

https://doi.org/10.1021/acs.analchem.3c02726
Anal. Chem. 2023, 95, 16593−16599

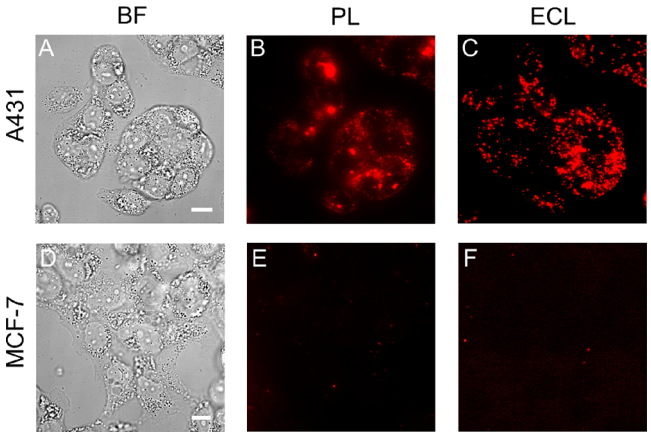

Figure 5. (A, D) BF, (B, E) PL, and (C, F) ECL images of EGFR on A431 and MCF-7 cells. Scale bars: 10 μm.

CONCLUSIONS

In conclusion, a confinement system for enhancing the cathodic ECL of $Ru(bpy)_3^{2+}$ has been successfully achieved by codoping $Ru(bpy)_3^{2+}$ and cathodic coreactant $S_2O_8^{2-}$ in silica nanoparticles with the help of cationic PDDA and the surfactant. The surfactant can efficiently encapsulate PDDA@$S_2O_8^{2-}$ and $Ru(bpy)_3^{2+}$ in a vesicle for the formation of silica nanoparticles, which show excellent modifiability with desirable groups. After surface amino modification and demulsification, the synthesized RuSSNs show 2.9-fold stronger ECL intensity than RuSNs/$S_2O_8^{2-}$ and 6-fold stronger cathodic ECL intensity than the $Ru(bpy)_3^{2+}/S_2O_8^{2-}$ system. Due to the better tolerance of live cells to cathodic potential stimulation than anodic stimulation, the self-enhanced cathodic ECL system has been successfully used for in situ ECL imaging of membrane protein EGFR on live cells with high sensitivity and good reliability. The proposed RuSSNs along with the confinement system provide a new paradigm for modulation of cathodic ECL emitters and ECL application in bioanalysis.

ASSOCIATED CONTENT

Supporting Information

The Supporting Information is available free of charge at https://pubs.acs.org/doi/10.1021/acs.analchem.3c02726.

Materials and reagents, apparatus, preparation of PDDA@$S_2O_8^{2-}$, AFM images and DPVs of RuSNs and RuSSNs, absorption spectra of $Ru(bpy)_3^{2+}$, RuSNs and RuSSNs, DPVs of $Ru(bpy)_3^{2+}$ in the presence of $K_2S_2O_8$, dependence of ECL intensity of RuSSNs/GCE on $K_2S_2O_8$ and PDDA concentrations and surface amination time, ECL stability of RuSSNs/GCE, photoluminescence spectra of Cy3-SA, RuSSNs, and Cy3-SA@RuSSNs, cell viability, BF, PL, and ECL images of EGFR on A431 cells, and amounts of Si, P, S, and Ru elements in RuSNs and RuSSNs (PDF)

AUTHOR INFORMATION

Corresponding Author

Huangxian Ju − *State Key Laboratory of Analytical Chemistry for Life Science, School of Chemistry and Chemical Engineering, Nanjing University, Nanjing 210023, P.R. China;* orcid.org/0000-0002-6741-5302; Phone: +86-25-89683593; Email: hxju@nju.edu.cn

Authors

Siqi Yu − *State Key Laboratory of Analytical Chemistry for Life Science, School of Chemistry and Chemical Engineering, Nanjing University, Nanjing 210023, P.R. China*

Xiangfu Hu − *State Key Laboratory of Analytical Chemistry for Life Science, School of Chemistry and Chemical Engineering, Nanjing University, Nanjing 210023, P.R. China*

Jianbin Pan − *State Key Laboratory of Analytical Chemistry for Life Science, School of Chemistry and Chemical Engineering, Nanjing University, Nanjing 210023, P.R. China*

Jianping Lei − *State Key Laboratory of Analytical Chemistry for Life Science, School of Chemistry and Chemical Engineering, Nanjing University, Nanjing 210023, P.R. China;* orcid.org/0000-0002-3594-180X

Complete contact information is available at: https://pubs.acs.org/10.1021/acs.analchem.3c02726

Notes

The authors declare no competing financial interest.

ACKNOWLEDGMENTS

We acknowledge the financial support of the National Natural Science Foundation of China (21890741 and 21827812) and the Science and Technology Project of Nanjing City (202110023).

REFERENCES

(1) Miao, W. *Chem. Rev.* **2008**, *108*, 2506−2553.
(2) Xu, L.; Li, Y.; Wu, S.; Liu, X.; Su, B. *Angew. Chem., Int. Ed.* **2012**, *51*, 8068−8072.
(3) Valenti, G.; Scarabino, S.; Goudeau, B.; Lesch, A.; Jović, M.; Villani, E.; Sentic, M.; Rapino, S.; Arbault, S.; Paolucci, F.; Sojic, N. *J. Am. Chem. Soc.* **2017**, *139*, 16830−16837.
(4) Voci, S.; Goudeau, B.; Valenti, G.; Lesch, A.; Jović, M.; Rapino, S.; Paolucci, F.; Arbault, S.; Sojic, N. *J. Am. Chem. Soc.* **2018**, *140*, 14753−14760.
(5) Zhang, J.; Jin, R.; Jiang, D.; Chen, H.-Y. *J. Am. Chem. Soc.* **2019**, *141*, 10294−10299.
(6) Chen, M.-M.; Xu, C.-H.; Zhao, W.; Xu, J.-J.; Chen, H.-Y. *J. Am. Chem. Soc.* **2021**, *143*, 18511−18518.
(7) Zhu, M.-J.; Pan, J.-B.; Wu, Z.-Q.; Gao, X.-Y.; Zhao, W.; Xia, X.-H.; Xu, J.-J.; Chen, H.-Y. *Angew. Chem., Int. Ed.* **2018**, *57*, 4010−4014.
(8) Wang, Y.; Guo, W.; Yang, Q.; Su, B. *J. Am. Chem. Soc.* **2020**, *142*, 1222−1226.
(9) Guo, W.; Ding, H.; Zhou, P.; Wang, Y.; Su, B. *Angew. Chem., Int. Ed.* **2020**, *59*, 6745−6749.
(10) Zanut, A.; Fiorani, A.; Canola, S.; Saito, T.; Ziebart, N.; Rapino, S.; Rebeccani, S.; Barbon, A.; Irie, T.; Josel, H. P.; Negri, F.; Marcaccio, M.; Windfuhr, M.; Imai, K.; Valenti, G.; Paolucci, F. *Nat. Commun.* **2020**, *11*, 2668.
(11) Zhu, W.; Dong, J.; Ruan, G.; Zhou, Y.; Feng, J. *Angew. Chem., Int. Ed.* **2023**, *62*, No. e202214419.
(12) Guo, W.; Zhou, P.; Sun, L.; Ding, H.; Su, B. *Angew. Chem., Int. Ed.* **2021**, *60*, 2089−2093.
(13) Liu, Y.; Zhang, H.; Li, B.; Liu, J.; Jiang, D.; Liu, B.; Sojic, N. *J. Am. Chem. Soc.* **2021**, *143*, 17910−17914.
(14) Ding, H.; Zhou, P.; Fu, W.; Ding, L.; Guo, W.; Su, B. *Angew. Chem., Int. Ed.* **2021**, *60*, 11769−11773.
(15) Ma, C.; Wu, S.; Zhou, Y.; Wei, H.-F.; Zhang, J.; Chen, Z.; Zhu, J.-J.; Lin, Y.; Zhu, W. *Angew. Chem., Int. Ed.* **2021**, *60*, 4907−4914.
(16) Li, B.; Huang, X.; Lu, Y.; Fan, Z.; Li, B.; Jiang, D.; Sojic, N.; Liu, B. *Adv. Sci.* **2022**, 2204715.
(17) Huang, X.; Li, B.; Lu, Y.; Liu, Y.; Wang, S.; Sojic, N.; Jiang, D.; Liu, B. *Angew. Chem., Int. Ed.* **2023**, *62*, No. e202215078.

(18) Lu, Y.; Huang, X.; Wang, S.; Li, B.; Liu, B. *ACS Nano* **2023**, *17*, 3809−3817.
(19) Dong, J.; Xu, Y.; Zhang, Z.; Feng, J. *Angew. Chem., Int. Ed.* **2022**, *61*, No. e202200187.
(20) Dong, J.; Lu, Y.; Xu, Y.; Chen, F.; Yang, J.; Chen, Y.; Feng, J. *Nature* **2021**, *596*, 244−249.
(21) Zhou, Y.; Dong, J.; Zhao, P.; Zhang, J.; Zheng, M.; Feng, J. *J. Am. Chem. Soc.* **2023**, *145*, 8947−8953.
(22) Liu, X.; Shi, L.; Niu, W.; Li, H.; Xu, G. *Angew. Chem., Int. Ed.* **2007**, *46*, 421−424.
(23) Chen, M.-M.; Cheng, S.-B.; Ji, K.; Gao, J.; Liu, Y.-L.; Wen, W.; Zhang, X.; Wang, S.; Huang, W.-H. *Chem. Sci.* **2019**, *10*, 6295−6303.
(24) Wang, N.; Gao, H.; Li, Y.; Li, G.; Chen, W.; Jin, Z.; Lei, J.; Wei, Q.; Ju, H. *Angew. Chem., Int. Ed.* **2021**, *60*, 197−201.
(25) Carrara, S.; Arcudi, F.; Prato, M.; De Cola, L. *Angew. Chem., Int. Ed.* **2017**, *56*, 4757−4761.
(26) Zhu, D.; Zhang, Y.; Bao, S.; Wang, N.; Yu, S.; Luo, R.; Ma, J.; Ju, H.; Lei, J. *J. Am. Chem. Soc.* **2021**, *143*, 3049−3053.
(27) Wang, T.; Wang, D.; Padelford, J. W.; Jiang, J.; Wang, G. *J. Am. Chem. Soc.* **2016**, *138*, 6380−6383.
(28) An, D.; Chen, Z.; Zheng, J.; Chen, S.; Wang, L.; Su, W. *Food Chem.* **2016**, *194*, 966−971.
(29) Chen, Y.; Gou, X.; Ma, C.; Jiang, D.; Zhu, J.-J. *Anal. Chem.* **2021**, *93*, 7682−7689.
(30) Irkham; Watanabe, T.; Fiorani, A.; Valenti, G.; Paolucci, F.; Einaga, Y. *J. Am. Chem. Soc.* **2016**, *138*, 15636−15641.
(31) Irkham; Fiorani, A.; Valenti, G.; Kamoshida, N.; Paolucci, F.; Einaga, Y. *J. Am. Chem. Soc.* **2020**, *142*, 1518−1525.
(32) Zanut, A.; Palomba, F.; Rossi Scota, M.; Rebeccani, S.; Marcaccio, M.; Genovese, D.; Rampazzo, E.; Valenti, G.; Paolucci, F.; Prodi, L. *Angew. Chem., Int. Ed.* **2020**, *59*, 21858−21863.
(33) Zanarini, S.; Rampazzo, E.; Ciana, L. D.; Marcaccio, M.; Marzocchi, E.; Montalti, M.; Paolucci, F.; Prodi, L. *J. Am. Chem. Soc.* **2009**, *131*, 2260−2267.
(34) Zanarini, S.; Rampazzo, E.; Bonacchi, S.; Juris, R.; Marcaccio, M.; Montalti, M.; Paolucci, F.; Prodi, L. *J. Am. Chem. Soc.* **2009**, *131*, 14208−14209.
(35) Climent, E.; Rurack, K. *Angew. Chem., Int. Ed.* **2021**, *60*, 26287−26297.
(36) Wang, L.; Yang, C.; Tan, W. *Nano Lett.* **2005**, *5*, 37−43.
(37) White, H. S.; Bard, A. J. *J. Am. Chem. Soc.* **1982**, *104*, 6891−6895.
(38) Gao, N.; Zeng, H.; Wang, X.; Zhang, Y.; Zhang, S.; Cui, R.; Zhang, M.; Mao, L. *Angew. Chem., Int. Ed.* **2022**, *61*, No. e202204485.
(39) Guo, W.; Ding, H.; Gu, C.; Liu, Y.; Jiang, X.; Su, B.; Shao, Y. *J. Am. Chem. Soc.* **2018**, *140*, 15904−15915.
(40) Nepomnyashchii, A. B.; Cho, S.; Rossky, P. J.; Bard, A. J. *J. Am. Chem. Soc.* **2010**, *132*, 17550−17559.
(41) Chiesa, M.; Giamello, E.; Che, M. *Chem. Rev.* **2010**, *110*, 1320−1347.
(42) Baselga, J.; Albanell, J. *Curr. Oncol. Rep.* **2002**, *4*, 317−324.
(43) Sugiyama, M. G.; Brown, A. I.; Vega-Lugo, J.; Borges, J. P.; Scott, A. M.; Jaqaman, K.; Fairn, G. D.; Antonescu, C. N. *Nat. Commun.* **2023**, *14*, 2681.

https://doi.org/10.1021/acs.analchem.3c02726
Anal. Chem. 2023, 95, 16593−16599